sions, wet/dry deposition, and sedimentation, are included and fully coupled with the meteorology. The aerosol types treated are marine, desert dust, carbonaceous, and sulfates. The aerosol model has been continuously upgraded since the completion of the 10-year reanalysis with the aim of increasing its forecast skill (see www.gmes-atmosphere.eu/services/aqac/global_verification/validation_reports). Since it was not possible to re-run the entire 2003–12 period of the MACC reanalysis, the most current model is used, including Global Fire Assimilation System (GFAS) biomass burning emissions (Kaiser et al. 2012), to produce an analysis for 2014. Here the focus is on the 2014 anomalies for carbonaceous aerosols because the desert dust and sea salt aerosol anomalies may be the result of model changes rather than real atmospheric signals. Plans for a new reanalysis under the Copernicus Atmosphere Monitoring Service are being made with a start date of summer 2016 and expected completion date of spring 2017.

Global maps of 2003–12 average carbonaceous AOD from the MACC-II reanalysis and the 2014 anomalies are shown in Fig. 2.41 and Plate 2.1v, respectively. Note the strong annual biomass burning signals in central Africa, South America, and Southeast Asia. In 2014 the carbonaceous AOD anomalies are strongly positive over Indonesia, North America, and Siberia. Figure 2.40 shows the 2014 anomalies for June–August (JJA) and September–November (SON), the seasons of intense regional biomass burning. The weak negative 2014 anomaly in biomass burning over South America, also observed in 2013, is likely connected to the decreasing trend in deforestation. The positive signal over central Africa is a persistent feature, but it is worth noting that this is a region of high biomass burning and the anomaly is relatively weak compared to those over North America and Siberia in JJA and over Indonesia in SON. The plume-shaped anomaly just east of Iceland in SON is due to the eruption of the Icelandic Bardarbunga–Holuhraun volcano, which appeared (spuriously) also in the carbonaceous aerosols.

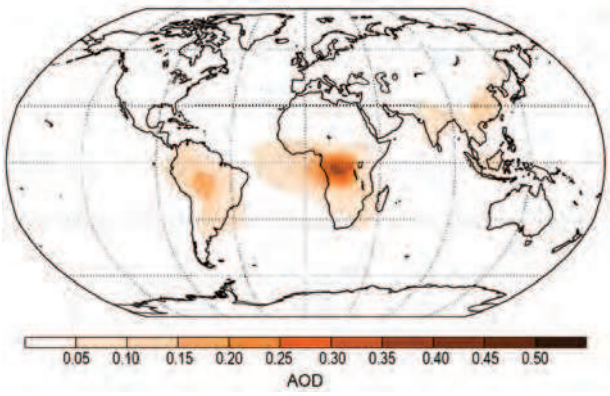

Fig. 2.41. Carbonaceous aerosol optical depth (AOD) average for 2003–12 from the MACC reanalysis.

4) Stratospheric ozone—M. Weber, W. Steinbrecht, C. Roth, M. Coldewey-Egbers, R. J. van der A, D. Degenstein, V. E. Fioletov, S. M. Frith, L. Froidevaux, C. S. Long, D. Loyola, and J. D. Wild.

Total ozone columns (TOCs) in 2014 exceeded the long-term (2000–12) average columns over much of the globe. One exception was the large region of negative anomalies extending eastwards from Greenland to northeastern Russia and southwards to the Black Sea (Plate 2.1t). Particularly large positive anomalies were observed in a zonal band near Antarctica with peak values >25 DU (Dobson units). Detailed discussions of Antarctic and Arctic ozone can be found in the Antarctic and Arctic chapters (sections 6g and 5c, respectively). The bands of positive ozone anomalies near 25° latitude in each hemisphere are a typical dynamical pattern caused by the easterly phase of the quasi-biennial oscillation (QBO).

Except in extreme cases of tropospheric ozone pollution, the total ozone column is a good surrogate for stratospheric ozone abundance because it is dominated by the much larger amounts of ozone in the stratosphere. Annual mean TOC anomalies at middle to polar latitudes in each hemisphere are largely determined by winter/spring ozone levels that vary considerably with stratospheric meteorological conditions (e.g., Steinbrecht et al. 2011; Weber et al. 2011). The 2014 negative anomalies at high Northern Hemisphere latitudes are due to low stratospheric ozone in the Arctic vortex, which was shifted towards the Eurasian sector, and transport from there to middle latitudes (Plate 2.1t; Fig. 2.42). In contrast, the positive TOC anomalies throughout the southern extratropics were caused by above-average stratospheric ozone from the weakly depleted 2014 Antarctic vortex (Fig. 2.42; see section 6h).

In Fig. 2.43 the TOC annual means from different data sources are shown for 1970–2014 in various zonal bands: near-global (60°S–60°N), middle latitudes in both hemispheres (35°–60°), and the inner tropics (20°S–20°N). The year-to-year variability in all ozone time series provides evidence of the QBO influence extending into the extratropics. The global average in 2014 is at the high end of the range of values observed since 2000. Figure 2.44 shows the upper stratospheric (40-km) ozone time series for the same zonal bands as Fig. 2.43. For most datasets the upper stratospheric ozone values in 2014 represent decadal maxima.

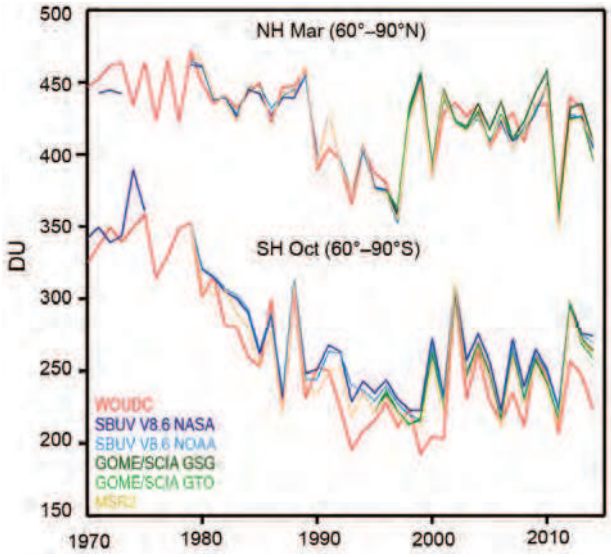

Fig. 2.42. Mar and Oct polar total column ozone in Dobson Units (DU) for the Northern and Southern Hemispheres, respectively. Data are from: WOUDC ground-based measurements combining Brewer, Dobson, SAOZ, and filter spectrometer data (red, Fioletov et al. 2002; 2008); the BUV/SBUV/SBUV2 V8.6 merged products of NASA (MOD V8.6, dark blue, McPeters et al. 2013; Chiou et al. 2014) and NOAA (light blue, Wild et al. 2012); and the GOME/SCIAMACHY/GOME-2 products GSG from University of Bremen (dark green, Kiesewetter et al. 2010; Weber et al. 2011) and GTO from ESA/DLR (light green, Loyola et al. 2009; Chiou et al. 2014). The MSR V2 (multi sensor reanalysis) combines various satellite data and algorithm versions after correction with respect to collocated WOUDC ground data in a data assimilation scheme (van der A et al. 2010; 2015). The MSR dataset was extended using GOME-2 total ozone. WOUDC values for 2014 are preliminary because not all ground station data were available in early 2015.

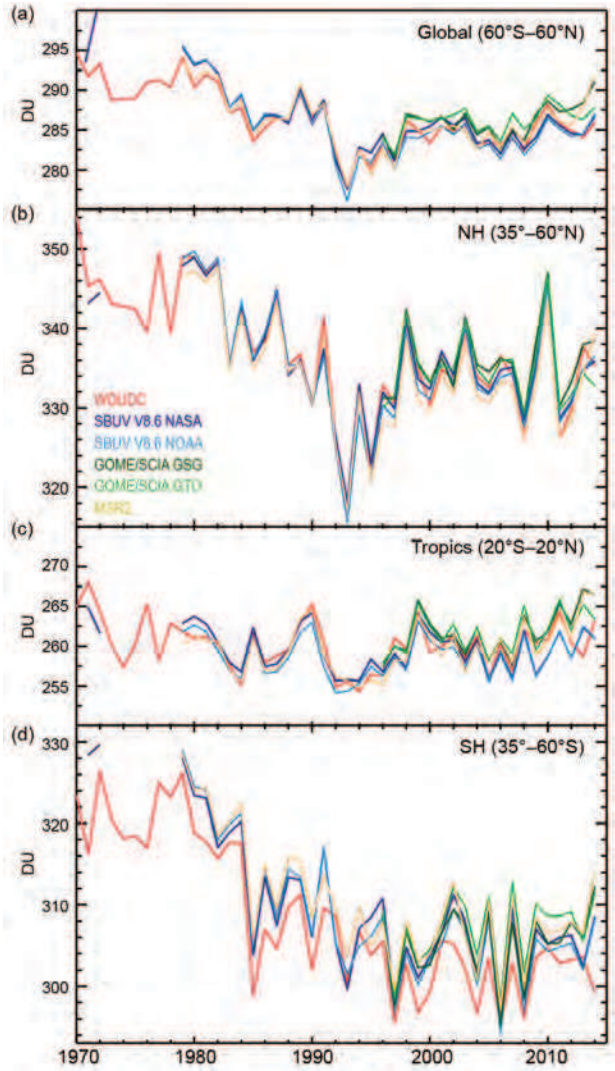

Fig. 2.43. Annual mean total ozone columns (DU) from 1970 to 2014 in four zonal bands: (a) 60°S–60°N (near-global), (b) 35°–60°N (NH midlatitudes), (c) 20°S–20°N (tropics), and (d) 35°–60°S (SH midlatitudes). Same data sources as in Fig. 2.42.

The recent WMO/UNEP ozone assessment (WMO 2014) provided an update on long-term ozone trends. It is clear that the Montreal Protocol and its Amendments were successful in ending the multi-decadal decline in stratospheric ozone by the late 1990s. A major question now is whether the decline in stratospheric chlorine observed since then has actually resulted in detectable ozone increases. The WMO assessment concluded that, at most latitudes, it is not yet possible to determine a statistically significant increase in total column ozone (lower stratosphere) because the expectedly small trends are masked by large interannual variability (Fig. 2.43; see also Chehade et al. 2014; Coldewey-Egbers et al. 2014). In the tropics no discernible long-term stratospheric trends have been observed for the entire 1970–2014 period. Note that trends in tropical tropospheric ozone can potentially mask stratospheric trends in tropical total columns (Shepherd et al. 2014) and there is evidence that decadal trends in the ENSO may have produced tropospheric ozone increases in some tropical regions during the past two decades (Coldewey-Egbers et al. 2014).

For trends in the vertical distribution of stratospheric ozone, however, the recent ozone assessment (WMO 2014) did conclude that the first signs of significant ozone increases are now detectible in the upper stratosphere. During 1979–97, stratospheric chlorine was increasing (Fig. 2.39a). Over the period 2000–13, stratospheric chlorine was decreasing. Before 1997 ozone had declined substantially in both the upper stratosphere (2 hPa, ~40 km) and lower stratosphere (50 hPa, ~20 km). The observed decline

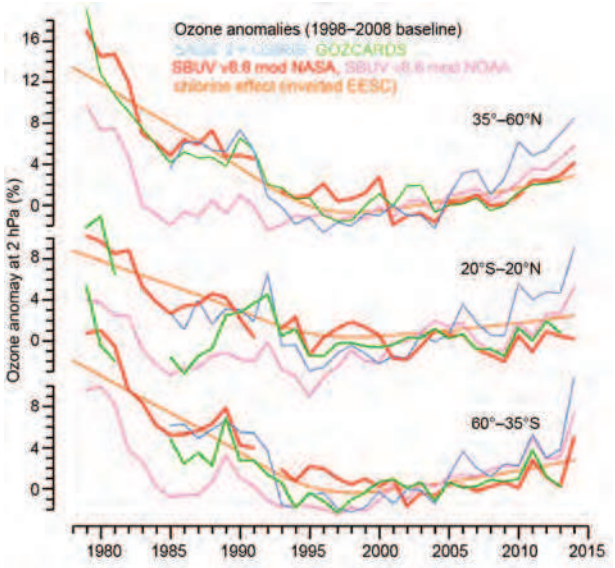

Fig. 2.44. Annual mean ozone anomalies at 2 hPa (~40 km, upper stratosphere) in three zonal bands. Data are from the merged SAGE II/OSIRIS (Bourassa et al. 2014), GOZCARDS (Froidevaux et al. 2015) and the BUV/SBUV/SBUV2 v8.6 merged products from NASA (McPeters et al. 2013) and NOAA (Wild et al. 2012). The orange curves are the EESC curves determined from a regression fit to the annual mean zonal mean including in addition factors representing QBO and the 11-year solar cycle (F10.7 solar radio flux).

is reproduced by chemistry climate model simulations (WMO 2011). The simulations demonstrate that the stratospheric ozone decline before 1997 was caused mainly by increasing chlorine and bromine, with some mitigation by greenhouse gas-induced stratospheric cooling that increased ozone production and slowed gas-phase ozone destruction cycles (WMO 2014).

Now that stratospheric chlorine and bromine are slowly decreasing, ozone is responding positively in the upper stratosphere. The increase is significant at 2 hPa (~40 km), and the observed and simulated trends are quite consistent. The model simulations indicate that about half of the ozone increase is due to declining chlorine loading and the other half is due to increasing emissions of greenhouse gases. Figure 2.44 demonstrates the success of the Montreal Protocol in turning ozone depletion into an ozone increase in the upper stratosphere. Detailed investigations of trends in ozone profiles (Tummon et al. 2015; WMO 2014, and references therein) were helpful to the assessment because they initiated additional iterations of satellite data processing and data merging, and brought together analyses of ground-based data (e.g., NDACC) and satellite data. Overall, the multiple analyses all support a current increasing trend in upper stratospheric ozone.

5) Stratospheric water vapor—S. M. Davis, K. H. Rosenlof, and D. F. Hurst

Throughout 2014 the anomalies of stratospheric water vapor (SWV) in the tropical lowermost stratosphere were moderately positive (wet) relative to the previous decade. In January 2014 the average tropical anomaly at 82 hPa was +0.4 ppmv (+10%; Figs. 2.45, 2.46a), in stark contrast to the strongly negative (dry) mean tropical anomaly of −0.7 ppmv (–20%) a year earlier (Hurst et al. 2014). The change in tropical lower SWV from January 2013 to January 2014 was +1.1 ppmv (+30%), ~50% of the typical seasonal amplitude at 82 hPa in the tropics. Strong water vapor increases in the tropical lower stratosphere during 2013–14 were observed at San José, Costa Rica (10°N), by balloon-borne frost point hygrometers (Fig. 2.47c) and throughout the equatorial belt by the *Aura* Microwave Limb Sounder (MLS, Fig. 2.45a). Although

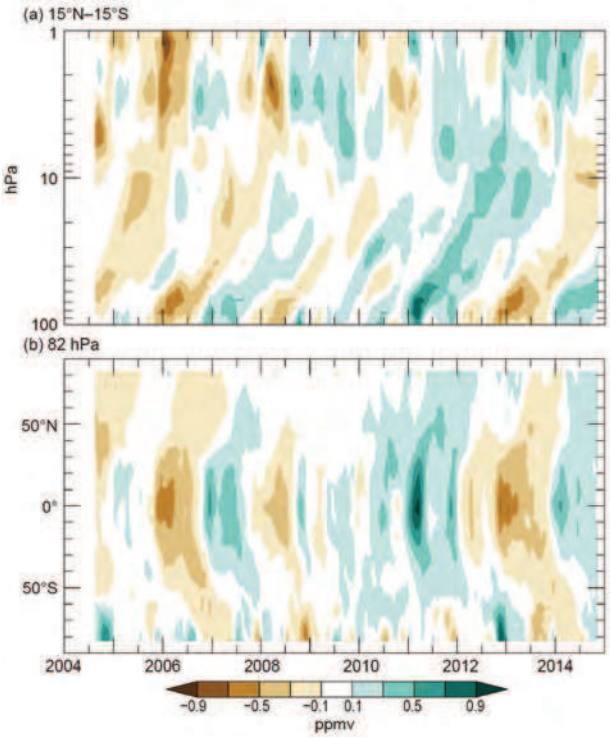

Fig. 2.45. (a) Vertical profiles of the MLS tropical (15°S–15°N) water vapor anomalies (ppmv) and (b) latitudinal distributions of MLS water vapor anomalies (ppmv) at 82 hPa (~18 km). Anomalies are differences from the mean 2004–14 water vapor mixing ratios for each month. (b) shows the propagation of tropical lower SWV anomalies to higher latitudes in both hemispheres as well as the influences of dehydrated air from the Antarctic polar vortex as it is transported to the southern midlatitudes.